Received: 14 December 2020 | Revised: 15 March 2021 | Accepted: 18 March 2021

DOI: 10.1002/hbm.25431

TECHNICAL REPORT

WILEY

Markov chain Monte Carlo methods for hierarchical clustering of dynamic causal models

Yu Yao[1] | Klaas E. Stephan[1,2]

[1]Translational Neuromodeling Unit (TNU), Institute for Biomedical Engineering, University of Zurich and ETH Zurich, Zurich, Switzerland

[2]Max Planck Institute for Metabolism Research, Cologne, Germany

Correspondence
Yu Yao, Translational Neuromodeling Unit (TNU), Institute for Biomedical Engineering, University of Zurich and ETH Zurich, Zurich, Switzerland.
Email: yao@biomed.ee.ethz.ch

Funding information
University of Zurich; René und Susanne Braginsky Foundation

Abstract

In this article, we address technical difficulties that arise when applying Markov chain Monte Carlo (MCMC) to hierarchical models designed to perform clustering in the space of latent parameters of subject-wise generative models. Specifically, we focus on the case where the subject-wise generative model is a dynamic causal model (DCM) for functional magnetic resonance imaging (fMRI) and clusters are defined in terms of effective brain connectivity. While an attractive approach for detecting mechanistically interpretable subgroups in heterogeneous populations, inverting such a hierarchical model represents a particularly challenging case, since DCM is often characterized by high posterior correlations between its parameters. In this context, standard MCMC schemes exhibit poor performance and extremely slow convergence. In this article, we investigate the properties of hierarchical clustering which lead to the observed failure of standard MCMC schemes and propose a solution designed to improve convergence but preserve computational complexity. Specifically, we introduce a class of proposal distributions which aims to capture the interdependencies between the parameters of the clustering and subject-wise generative models and helps to reduce random walk behaviour of the MCMC scheme. Critically, these proposal distributions only introduce a single hyperparameter that needs to be tuned to achieve good performance. For validation, we apply our proposed solution to synthetic and real-world datasets and also compare it, in terms of computational complexity and performance, to Hamiltonian Monte Carlo (HMC), a state-of-the-art Monte Carlo technique. Our results indicate that, for the specific application domain considered here, our proposed solution shows good convergence performance and superior runtime compared to HMC.

KEYWORDS
computational psychiatry, functional magnetic resonance imaging, generative embedding, Markov chain Monte Carlo sampling, model inversion

1 | INTRODUCTION

Dealing with the heterogeneity in clinical populations represents an important challenge for neuroimaging. This is particularly the case for psychiatry where contemporary diagnostic classifications group together patients with presumably heterogeneous disease mechanisms (Owen, 2014; Stephan et al., 2016). This heterogeneity is one possible reason for the low success rate of clinical trials, and stratification (e.g., by clustering the population into specific subgroups) might considerably increase the power of clinical trials (Schumann

et al., 2014). This is a particularly promising approach when such clusters or subgroups are not defined in terms of abstract data features, but are interpretable in terms of disease-relevant mechanisms (Stephan et al., 2016).

This technical note addresses the specific problem of applying Markov chain Monte Carlo (MCMC) to hierarchical clustering in the context of generative embedding (GE). GE refers to a mapping from data to feature space that is instantiated by a generative model (Brodersen et al., 2011). Put simply, GE boils down to using (a function of) posterior densities of model parameters in order to define a feature space for subsequent machine learning. By achieving theory-led dimensionality reduction jointly with interpretability of features (in terms of data-generating mechanisms embodied by the generative model), GE can both enhance the performance and interpretability of machine learning when applied to neuroimaging or behavioural data (for reviews, see Frässle et al., 2018; Stephan et al., 2017). However, the necessity of model inversion can make GE technically challenging, particularly in hierarchical settings.

Here, we deal with the hierarchical unsupervised case of GE, that is, group-level clustering in a high-dimensional space of latent variables. More specifically, this article deals with the challenge of inverting a hierarchically structured generative model that distinguishes clusters of latent parameters from other (subject-wise) generative models, the (equally latent) dynamics of processes governed by these parameters, and the observations resulting from these processes. Specifically, we focus on hierarchical unsupervised GE (HUGE, Yao et al., 2018) where the cluster formulation is based on Gaussian mixture models and the subject-wise generative model is a dynamic causal model (DCM). DCM is a nonlinear dynamic system model for estimating effective (directed) brain connectivity from fMRI (Friston, Harrison, & Penny, 2003) or electroencephalography/magnetoencephalography (EEG/MEG) data (David et al., 2006). Like almost any other biological dynamic system model (cf. Gutenkunst et al., 2007), it may exhibit high posterior correlations among some of its parameters (Stephan, Weiskopf, Drysdale, Robinson, & Friston, 2007), rendering model inversion a difficult task.

Such challenges associated with parameter estimation are not unique to dynamic system models of neuroimaging data. Generally, dynamic system models are popular in scientific areas—including systems biology, medicine and neuroscience—that require an understanding of complex data in terms of latent parameters that govern the evolution of observed timeseries. Their application has been aided by the development of a variety of model inversion methods based on Hamiltonian Monte Carlo (HMC, Calderhead & Girolami, 2011; Kramer, Calderhead, & Radde, 2014), MCMC (Xun, Cao, Mallick, Maity, & Carroll, 2013), variational inference (VI, Friston, Mattout, Trujillo-Barreto, Ashburner, & Penny, 2007; Meeds, Roeder, Grant, Phillips, & Dalchau, 2019), or gradient matching techniques (Calderhead, Girolami, & Lawrence, 2009; Wenk et al., 2019).

However, incorporating a dynamic systems model, such as DCM, into a hierarchical clustering model exacerbates the difficulties associated with model inversion due to the interaction between the estimation of the parameters of the DCM and the clustering model. In particular, standard MCMC methods display a tendency to fail to converge under these circumstances, an issue we address in this article. The contributions of this article are as follows. First, we identify key features in the structure of the hierarchical clustering model which contribute to the convergence issues observed with MCMC. Based on these insights, we then propose a heuristic solution tailored to hierarchical clustering, which aims to improve convergence while preserving computational complexity. We demonstrate the effectiveness of our solution on synthetic and real-world examples based on a hierarchical clustering model for DCM known as HUGE (Yao et al., 2018). Finally, we discuss the complexity and performance of our proposed solution in comparison to HMC, an advanced, general purpose Monte Carlo method designed to solve the convergence issues of standard MCMC methods without relying on detailed knowledge of the specific application.

Our work significantly goes beyond previous work on parameter estimation for hierarchically structured generative models. For example, Raman, Deserno, Schlagenhauf, and Stephan (2016) used standard MCMC in an early version of the HUGE model, but did not provide a detailed analysis on speed of convergence or computational complexity. The same model is also discussed in Yao et al. (2018), who applied VI instead of MCMC. Despite being extremely efficient, VI suffers from a number of drawbacks, making the availability of a complementary MCMC-based inversion scheme desirable. Specifically, VI traditionally requires the use of conjugate priors, which may restrict the expressiveness of the model and makes model extensions difficult. In addition, the simplifying assumptions on the approximate posterior required for VI mean that VI lacks both the asymptotic exactness and the ability to approximate multi-modal posteriors afforded by MCMC. Other hierarchically structured generative models of dynamic systems include the parametric empirical Bayesian variant of DCM (Friston et al., 2016) and hierarchically structured dynamic system models for applications in system biology (Meeds et al., 2019). However, in the latter two models, assignments of data points to groups are not inferred, but have to be supplied with the data; these models can therefore only be used for supervised learning (see also Ahn, Haines, & Zhang, 2017).

The application of HMC to hierarchical models in general has been discussed in Betancourt and Girolami (2015). In the present paper, we focus on the combination of a hierarchical model structure with a dynamic systems model. In addition, we take a different approach to model inversion by attempting to augment standard MCMC with specialized proposal distributions. In this context, we will provide a detailed comparison of our proposed approach with HMC.

2 | METHODS

2.1 | MCMC for hierarchical clustering

In hierarchical clustering, a group-level clustering model (such as a Gaussian mixture model in the case of HUGE) is combined with a subject-wise generative model in such a way that the generative

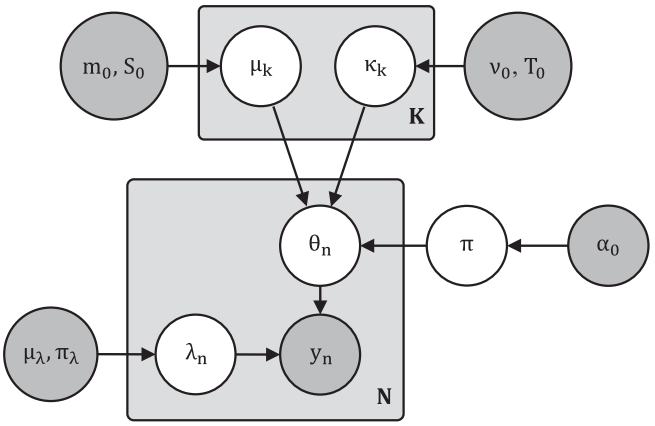

FIGURE 1 Graphical model for the hierarchical clustering problem

model is used to fit the subject-specific data points, while the clustering model is used to cluster the estimates of the latent parameters of the subject-wise generative models. Figure 1 shows the graphical model of this hierarchical clustering problem with K clusters and N subjects, which contains the HUGE model as a special case. For each of the $n = 1, \ldots, N$ subjects, θ_n represents the parameters of the generative model that connects the subject-specific data y_n with the clustering model. Here, the clustering model is represented by a Gaussian mixture model, where cluster number k ($1 \le k \le K$) is described by its mean μ_k and log-precision κ_k and is assigned a cluster weight $\pi[k]$. λ_n denotes the precision of observation noise. Note that despite having a fixed number of clusters K, the model can accommodate clustering solutions with less than K cluster, by leaving some of the clusters empty. Hence, K should be viewed as an upper limit on the number of clusters expected in the dataset. This stands in contrast to traditional clustering methods like k-means.

Assuming that the observation model can be expressed as a, possibly nonlinear, transformation $g(\cdot)$ with additive Gaussian noise:

$$y_n = g(\theta_n) + \epsilon, \text{with } \epsilon \sim N(0, exp(-\lambda_n)), \tag{1}$$

we can express the joint distribution of the hierarchical clustering model as follows:

$$p(y_n, \theta_n, \lambda_n, \mu_k, \kappa_k, \pi) = D\left(\pi|\alpha_0\right) \prod_{k=1}^{K} \left\{ N\left(\mu_k|m_0, S_0\right) N\left(\kappa_k|\nu_0, T_0^{-1}\right) \right\} \times$$

$$\prod_{n=1}^{N} \left\{ N\left(y_n|g(\theta_n), exp(-\lambda_n)\right) N\left(\lambda_n|\mu_\lambda, \pi_\lambda^{-1}\right) \sum_{k=1}^{K} \pi[k] N(\theta_n|\mu_k, exp(-\kappa_k)) \right\}, \tag{2}$$

where the symbols $N(\cdot)$ and $D(\cdot)$ denote the multivariate Normal and Dirichlet distributions, respectively. In addition, α_0 denotes the parameter of the prior over cluster weights, m_0 and S_0 the prior mean and covariance of the cluster centres and ν_0 and T_0 the prior mean and covariance of the cluster log-precision.

Performing Bayesian inference on this model requires the joint estimation of the parameters of the subject-wise generative models (θ_n and λ_n) and the parameters of the group-level clustering model (μ_k, κ_k, and π). In principle, an attractive way to do this is to apply Monte Carlo sampling, which offers a number of advantages including asymptotic exactness, lack of conjugacy requirements, and the availability of well-established standard algorithms and software tools. One of these standard algorithms is Metropolized Gibbs sampling, which can be applied almost universally to any target distribution which can be evaluated up to a multiplicative constant for arbitrary parameter combinations (Gelman, 2014). It works by sampling parameters, or groups of parameters, in turn from their conditional distribution given the remaining parameters of the model, employing the Metropolis–Hastings (MH) algorithm whenever it is not possible to sample from one of the conditional distributions directly. Specifically, for hierarchical clustering, this means sampling each of the following parameters θ_n, λ_n, μ_k, κ_k, and π ($1 \le n \le N$, $1 \le k \le K$) from its conditional distribution given all the remaining parameters, which is done using MH, due to the lack of conjugacy. The exact forms of these conditional distributions are given in the Supplementary Material.

However, a major weakness of Gibbs sampling in particular, and MH in general, is slow convergence in the case of highly correlated parameters (Bishop, 2006). In our case, the structure of hierarchical clustering induces a strong correlation between the parameters of the clustering model, specifically μ_k, and the parameters of the generative model θ_n. This can be understood by noting that μ_k is the parent of θ_n in the graphical model in Figure 1. Additionally, the parameters μ_k, κ_k, and π are strongly anti-correlated, as they are co-parents of θ_n. Note that despite being nominally unobserved, we are conditioning on the current sample value of θ_n when drawing the parents during Gibbs sampling. Hence, these variables suffer from the well-known "explaining away" effect (Bishop, 2006).

When applying Gibbs sampling to hierarchical clustering in practice, these issues lead to very characteristic failure modes where either some data points are stuck in the wrong cluster, or an empty (or almost empty) cluster is stuck close to the prior mean m_0. These issues are exacerbated by generative models $g(\theta_n)$ with high posterior correlations among their parameters; an issue that is frequently found in generative models involving dynamical system formulations, such as DCM. Examples illustrating these failure modes are provided in Section 3.

In order to address convergence issues, advanced sampling methods have been developed. HMC (Betancourt & Girolami, 2015; Calderhead & Girolami, 2009; Duane, Kennedy, Pendleton, & Roweth, 1987) is generally considered to be the state-of-the-art in this field, designed to increase sampling efficiency and speed up convergence for a wide range of target distributions. However, this generality comes at the cost of higher complexity, both numerically and in terms of implementation effort. In addition, it introduces the need to tune additional hyperparameters to achieve optimal performance (Behrens, Friel, & Hurn, 2012; Betancourt, 2016). In the following section, we introduce an alternative solution with the goal of improving convergence of the Metropolized Gibbs sampler for hierarchical clustering, while minimising the additional computational complexity.

2.2 | Improving convergence for hierarchical clustering

In the previous section, we have identified key features in hierarchically structured clustering models which are responsible for convergence issues in MCMC-based inversion of these models. In order to address these issues, we suggest constructing specialized proposal distributions tailored to the dependency structure of the hierarchical clustering model.

Specifically, we suggest using special proposal distributions during the MH phase of the Metropolized Gibbs sampler which depend on the sample value of the parameters which are not being sampled at the current step. For example, when sampling from the conditional distribution over cluster means μ_k given all remaining parameters, one may use a proposal distribution which depends on the current sample value of the other parameters (in the following, the (τ) in the exponent denotes the current sample value, while the star in the exponent denotes the proposal value):

$$q\left(\mu_k^*\right) = q\left(\mu_k^* | \theta_n^{(\tau)}, \pi^{(\tau)}, \ldots\right), \tag{3}$$

This departs from standard proposal distributions, such as using a Gaussian kernel centred on the last sample value of μ_k itself:

$$q\left(\mu_k^*\right) = N\left(\mu_k^* \middle| \mu_k^{(\tau)}, \sigma_{\mathrm{MH}}\right). \tag{4}$$

Note that our idea does not violate detailed balance since the target distribution is the conditional distribution, and we only use the sample values of the parameters we are currently conditioning on.

In theory, the optimal choice for such a proposal distribution would be the conditional distribution itself. However, the inability to sample from the conditional distribution directly is what necessitated the MH step in the first place. In practice, we therefore alternate between (a) a standard proposal distribution, like a Gaussian kernel centred on the last sample, which is used to explore the current posterior mode, and (b) a special proposal distribution, designed to disrupt the random walk behaviour of the chain, for example, by proposing jumps to possible locations of other modes of the posterior. The key is that these special proposal distributions should be more effective if they are informed by the current sample value of the other parameters. Note that alternating between different transition operators in MH is valid, as long as each individual transition operator is valid (Brooks, Gelman, Jones, & Meng, 2011).

The idea of disrupting random walk behaviour in MH using specialized proposal distributions—for example, derived from extensive domain knowledge—is not new. In fact, our approach was inspired by Carlin and Chib (1995) who, after reformulating a model selection problem in terms of a clustering model, faced convergence issues similar to those seen in hierarchical clustering. However, what distinguishes our approach from previous methods is the insight that, in the case of hierarchical clustering, the special proposal distributions can make use of the sample value of the parameters currently not being sampled to identify promising proposals. For example, when sampling from the conditional distribution over clustering parameters, one may use a proposal distribution informed by the current sample value of the subject-level parameters. This eliminates the need for designing proposal distributions based on domain knowledge, making the method less application dependent. In addition, it also eliminates the need for tuning the special proposal distribution in preliminary test runs of the sampler, as was done by Carlin and Chib (1995).

Based on the issues with hierarchical clustering identified in the previous section, we focus on two steps in the Metropolized Gibbs sampler: (a) sampling from the conditional distribution over θ_n and (b) sampling from the conditional distribution over the cluster parameters π, μ_k, and κ_k.

For Step (a), our special proposal distribution is extremely simple: sample the proposal θ_n^* randomly from the clustering model:

$$q\left(\theta_n^*\right) = \sum_{k=1}^{K} \pi^{(\tau)}[k] N\left(\theta_n^* \middle| \mu_k^{(\tau)}, \exp\left(-\kappa_k^{(\tau)}\right)\right), \tag{5}$$

In order to satisfy detailed balance, we need to derive the corresponding MH acceptance rate, which is given by:

$$a = \min\left\{1, \frac{p\left(\theta_n^*\right) q\left(\theta_n^{(\tau)} | \pi^{(\tau)}, \mu_k^{(\tau)}, \kappa_k^{(\tau)}\right)}{p\left(\theta_n^{(\tau)}\right) q\left(\theta_n^* | \pi^{(\tau)}, \mu_k^{(\tau)}, \kappa_k^{(\tau)}\right)}\right\}. \tag{6}$$

Inserting the expressions for the conditional distribution (see Equation (S5) in the Supplementary Material) and the proposal distribution from Equation (5), the acceptance ratio simplifies to the ratio of likelihoods, since all terms depending on the cluster parameters cancel out:

$$a = \min\left\{1, N\left(\frac{y_n \middle| g\left(\theta_n^*\right), \exp\left(-\lambda_n^{(\tau)}\right)\right)}{N\left(y_n \middle| g\left(\theta_n^{(\tau)}\right), \exp\left(-\lambda_n\right)\right)}\right\}. \tag{7}$$

Therefore, this kernel has the convenient property that it has no free hyperparameters which need to be tuned. In fact, the only parameter that needs to be tuned in the entire approach is the frequency with which to propose from this distribution as compared to the standard Gaussian kernel. In the experiments presented in Section 3, this frequency was chosen during a preliminary test run of the sampler and kept fixed for all subsequent experiments. This was done in order to keep the setup as simple as possible. However, the tuning process can in principle be accomplished during the burn-in phase of the sampler, removing the need for any preliminary test runs.

The second special proposal density (step (b) above) was designed to address the problem of transitioning between different posterior modes. Specifically, this proposal jointly samples cluster model parameters π, μ_k, and κ_k given the current sample values of θ_n, while allowing transitions between posterior modes associated with different number of clusters. This is achieved using the following process. First, we

sample a number k uniformly between 1 and K, where K is the maximum number of clusters in the model. Then, we use k-means to identify a plausible clustering solution with exactly k clusters and draw the parameters, that is, weight, mean and covariance, of the first k clusters from a distribution centred on this solution. Finally, if k is smaller than K, the parameters of the remaining clusters from k + 1 to K are sampled from the prior over clusters. The last step ensures that the overall number of parameters stays constant, avoiding the complications arising from changing the dimensionality of the parameter space (Green, 1995).

Given that this proposal density requires the use of k-means to obtain an intermediate clustering solution, it may appear that considerable computational overhead is being introduced. However, our experiments in Section 3 show that the computational cost introduced by our special proposal distributions is almost negligible. The derivation of the acceptance ratio for this proposal distribution can be found in the Supplementary Material. The key feature of this proposal is that it allows transitions between posterior modes representing clustering solutions with different number of clusters. For example, in certain situations, the solution where all data points belong to one big cluster might be equally plausible as the solution where data points are divided into two smaller clusters. Transitioning between these two solutions is extremely difficult for standard Gibbs sampling, but is possible with the proposal density introduced above.

Also, note that the proposal introduced above makes a joint update to cluster weights, means and covariances. This is in contrast to standard Gibbs sampling, where these variables are sampled successively from their respective conditional distributions. This makes the standard Gibbs sampling susceptible to the strong posterior correlations between these parameters.

In Section 3, we present empirical evidence that our proposed approach significantly improves convergence for hierarchical clustering while avoiding the added complexity of advanced Monte Carlo schemes. To this end, we apply our method to a hierarchical clustering model built on a subject-specific generative model of effective brain connectivity; the latter, a DCM of fMRI data is briefly introduced in the next section.

2.3 | Dynamic causal modelling

The approach introduced in Section 2.2 applies to hierarchical clustering, irrespective of the subject-specific generative model. However, for the remainder of this article, we will focus on a hierarchical clustering model known as HUGE (Yao et al., 2018), which combines clustering with a class of dynamic systems models called DCM. In the following, we provide a short introduction to DCM; specifically, its implementation for fMRI data. For a more detailed description of DCM for fMRI, we refer to the original paper by Friston et al. (2003).

DCM is a class of generative models for inferring effective connectivity between brain regions from fMRI data (Friston et al., 2003) or EEG or MEG data (David et al., 2006). A DCM for fMRI consists of an evolution function (formulated as a bilinear or non-linear dynamic systems model) which is linked to a nonlinear observation function. Specifically, the evolution function $f(\cdot)$ describes the temporal evolution of neuronal population states x in a network of brain regions, together with the evolution of activity-induced hemodynamic states s:

$$(\dot{x},\dot{s})^T = f(x(t),s(t),u(t)) \tag{8}$$

The evolution function is parameterized by parameters θ (see below) and under the influence of known perturbations or external inputs u. These inputs u could represent, for example, sensory stimuli or cognitive interventions (such as cued attention).

Neuronal and hemodynamic states are linked via a nonlinear observation function $h(\cdot)$ to the observed fMRI data $y(t) = h(x(t), s(t)) + e(t)$, under Gaussian assumptions about the noise (and dealing with non-IID properties). For simplicity, this description ignores region-specific parameters of this observation function; for more details on the hemodynamic model, we refer to Friston, Mechelli, Turner, and Price (2000) and Stephan et al. (2007).

Of particular interest for practical applications is the parameterization of the neuronal evolution function, that is, the part of $f(\cdot)$ which describes the evolution of the neuronal activity x, consisting of a bilinear evolution function with parameter matrices A, C and the set $B = \{B^{(l)} : l = 1, \ldots, L\}$ containing one matrix per input:

$$\dot{x} = Ax + \sum_{l=1}^{L} u_l B^{(l)} x + Cu \tag{9}$$

Here, A represents the endogenous connectivity, that is, the connectivity between regions in the absence of external influences. $B^{(l)}$ represents the modulatory influence of input l on the endogenous connectivity in A. And finally, C represents the strength of inputs that drive the regions directly.

Evaluation of DCM as a generative model requires numerical integration of the evolution function f, which, assuming the use of an efficient integrator like the Euler method, requires $O(TLR^2)$ operations, where R denotes the number of regions and T the length of the fMRI time series. In comparison, the complexity of evaluating the observation function h is negligible. Note also that in contrast to other domains which apply dynamic system models (Kramer et al., 2014), the process of fitting DCM to neuroimaging data is mostly driven by transients and less by the steady-state.

When using DCM as the subject-wise generative model in hierarchical clustering, the model parameters of interest would be represented by $\theta = \{A, B, C\}$, while the predicted fMRI time series result from the process of first integrating the DCM evolution equation $f(\cdot)$ and then applying the observation function $h(\cdot)$.

2.4 | Hamiltonian Monte Carlo

HMC is considered to be the state-of-the-art in the field of general purpose Monte Carlo sampler capable of avoiding random walk behaviour and obtaining less correlated samples. However, the efficiency of HMC comes at the cost of increased computational

complexity per sample, which may offset the benefit of being able to use shorter chains. This is because in order to obtain a new sample, HMC needs to simulate Hamiltonian dynamics in a potential landscape defined by the target distribution, which requires numerically integrating a dynamical system (Brooks et al., 2011). In this section, we present a theoretical analysis of the complexity of HMC for hierarchical clustering models of DCM in comparison with more conventional sampling techniques.

Theoretical analysis shows that the complexity of HMC of $O(D^{5/4})$ compares favourably to the complexity of basic methods, such as Gibbs sampling, of $O(D^2)$ (Hoffman & Gelman, 2014), where D denotes the dimensionality of the parameter space. However, this complexity refers to the number of samples needed to explore the target distribution and does not account for the complexity of obtaining each sample. On a sample-by-sample level, HMC introduces two sources of additional complexity: the evaluation of gradients of the target distribution and the simulation of the Hamiltonian dynamics. While gradient evaluation may be addressed with automatic differentiation techniques without increasing the order of numerical complexity (Baydin, Pearlmutter, Radul, & Siskind, 2018), simulating the Hamiltonian dynamics requires a symplectic integration scheme such as the leapfrog integrator (Brooks et al., 2011), which needs two evaluations of the gradient of the target density per integration step.

Unfortunately, in a dynamic systems model, such as DCM, evaluation of the joint distribution and the associated gradients is often the most expensive part. For DCM, the complexity of a single evaluation is given by $O(TLR^2)$. Hence, evaluating the joint distribution for a DCM-based hierarchical clustering model, such as HUGE, with data from N subjects would require on the order of $O(TNLR^2)$ operations due to the DCM part of the model alone. At the same time, the number of parameters of such a model is approximately given by $D = (N+K)LR^2 \approx NLR^2$ (assuming $N \gg K$). This means that the evaluation of the joint distribution alone would contribute $O(TD)$ and $O(JTD)$ operations to Gibbs sampling and HMC, respectively, where J denotes the number of steps used by the leapfrog integrator in HMC.

The optimum value for J depends on the structure of the target distribution itself and is difficult to determine a priori (Betancourt, 2016). However, for typical DCMs, the length of the fMRI time series T is approximately on the same order as LR^2 (Friston et al., 2003). Hence, it becomes clear that the cost of evaluating the DCM could very well dominate the complexity of the entire inference algorithm, and may even negate the advantage afforded by HMC in terms of providing more independent samples if JT is of the same magnitude as D.

In the next section, we investigate this problem from an empirical perspective by comparing the performance and computation time of HMC and Metropolized Gibbs sampling on a set of synthetic and real-world datasets.

3 | RESULTS

In this section, we present results from two experiments which illustrate the convergence issues encountered with standard Gibbs sampling for hierarchical clustering, as well as the improvements achieved using the approach proposed in Section 2.2. For comparison, we also ran both experiments using HMC. For this purpose, we chose the No-U-Turn sampler provided by stan (Stan Development Team, 2020), because of its ability to automatically tune the hyperparameters of HMC for optimal performance. The code used to run these experiments will be made available as part of the open-source toolbox TAPAS (Translational Neuromodeling Unit, 2014). To account for issues related to label switching, samples were relabelled with the approach from Stephens (2000) throughout all our experiments. This method was chosen because it unifies several previously established relabeling schemes for MCMC. Details on the computing environment can be found in the Supplementary Material.

Since the goal of this technical report is the development of an efficient method for improving convergence of Gibbs sampling for hierarchal clustering, we focus our quantitative analysis on the assessment of the convergence of the samplers and the correctness of the inference for synthetic data with available ground truth. While convergence is assessed using the potential scale reduction factor (PSRF) proposed by Brooks and Gelman (1998), the quality of inference can be most conveniently summarized by calculating the balanced purity (Brodersen et al., 2014) of the clustering result. Although it may seem tempting to use a measure such as the root mean squared (RMS) error of the posterior mean of the DCM parameters, it should be noted that, for models with high posterior covariance between its parameters, such as DCM, the posterior may extend over a larger area or even be multi-modal, rendering the posterior mean less informative. In most circumstances, an RMS-based measure would likely reflect the posterior covariance of the model instead of the accuracy of the inversion scheme. However, since we are dealing with a generative model, it is possible to analyse model fit by visualising samples from the posterior over the predicted BOLD signal. In the following, we provide a short introduction to the PSRF and the balanced accuracy.

The PSRF was introduced by Brooks and Gelman (1998) in order to assess the convergence of MCMC samplers. It quantifies the consistency between independent chains by comparing the variance of the samples within each chain with the variance of samples between chains. Given m chains each containing n samples, the PSRF is calculated via the formula:

$$\hat{r} = \frac{m+1}{m}\frac{\hat{\sigma}_+^2}{W} - \frac{n-1}{mn} \text{ with } \hat{\sigma}_+^2 = \frac{n-1}{n}W + \frac{B}{n}, \tag{10}$$

where W and B/n denote the within-chain variance and between-chain variance, respectively. Upon convergence, the PSRF should approach a value of 1. In experimental settings, a value between 1 and 1.1 is generally accepted to indicate convergence of the sampler.

The balanced purity (Brodersen et al., 2014) is a measure of the quality of clustering solutions, where a value of 1 indicates a perfect result, while a value of 0.5 indicates random assignment (for $K = 2$). Given estimated $\Omega = (\omega_1, \ldots, \omega_K)$ and true $C = (c_1, \ldots, c_J)$ class

assignments, the balanced purity is calculated from the purity using the formula:

$$bp(\Omega,C) = \left(1-\frac{1}{K}\right)\left(\frac{purity(\Omega,C)-\xi}{1-\xi}\right)+\frac{1}{K} \quad (11)$$

where ξ is the degree of imbalance (i.e., the fraction of subject associated with the largest class) and the purity is defined as:

$$purity(\Omega,C) = \frac{1}{N}\sum_{k=1}^{K} \max_j |\omega_k \cap c_j|. \quad (12)$$

Here, $|\omega_k \cap c_j|$ denotes the number of subjects in cluster k which are associated with the true class j. The advantage of using the balanced purity score is that it accounts for the biasing effects of an imbalanced dataset, which affects the usefulness of the more traditional purity score in dataset containing classes of varying sizes.

3.1 | Experiment 1: Synthetic data

In the first experiment, we used synthetic data with known ground truth to validate and compare the different inversion methods. For this purpose, we generated 20 synthetic datasets, where each dataset contained 30 simulated subjects divided into two clusters with different patterns of network connectivity. Repeating the experiment for 20 datasets introduces a range of variations which ensures that any observed differences between the samplers are not simply due to random properties of a particular dataset.

The time series data of each subject were generated using the three-region DCM shown in Figure 2a with connectivity parameters drawn randomly from a Gaussian distribution centred on the respective cluster mean. The cluster means were chosen to represent the two distinct connectivity patterns shown in Figure 2b,c. The structure of this DCM was inspired by an actual experimental design from van Leeuwen, den Ouden, and Hagoort (2011). The numerical values of the ground truth parameters are listed in the Supplementary Material.

For each dataset, we inverted the HUGE model using 3 different approaches: standard Metropolized Gibbs sampling, the improved version described in Section 2, and HMC as implemented in stan. For the Gibbs samplers, four independent chains with 1×10^5 samples each were run, which took less than 3.5 hr on average. The first half of each chain was discarded for burn-in before convergence was assessed using the PSRF.

Figure 3 (top panels) shows plots of the PSRF values of the model parameters of HUGE across all synthetic datasets. Each dot represents the PSRF value of one model parameter of HUGE for one of the 20 synthetic datasets. Model parameters include subject-level DCM parameters, measurement noise precision, cluster mean and variance and cluster weights. The PSRF values for our improved Gibbs sampler are mostly within the range of 1–1.1 which is generally accepted to indicate convergence of the sampler. However, for the standard Gibbs sampler, the PSRF values indicate failure of convergence for some of the datasets. This impression is confirmed by Figure 4, showing

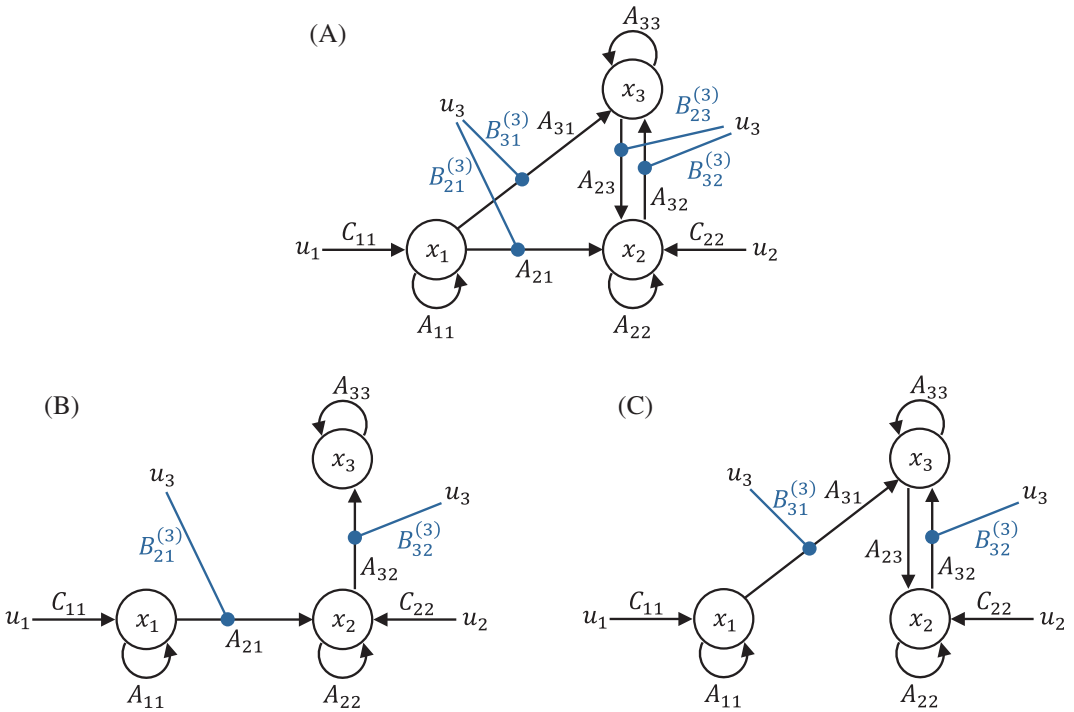

FIGURE 2 (a) Dynamic causal model (DCM) network for generating synthetic datasets. (b) Sub-network corresponding to the first cluster. (c) Sub-network corresponding to the second cluster

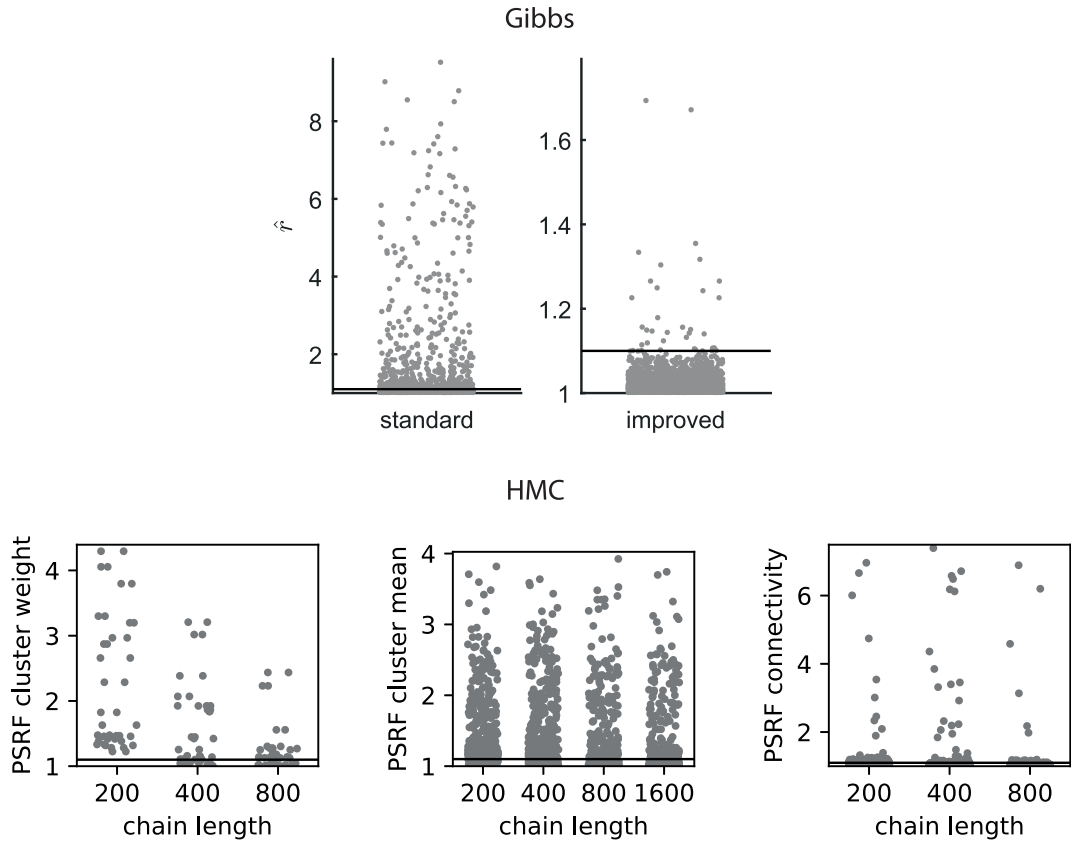

FIGURE 3 Top: Range of potential scale reduction factor (PSRF) of standard and improved Gibbs sampling observed across all synthetic datasets. Bottom: Range of PSRF values for different sets of parameters obtained with Hamiltonian Monte Carlo (HMC) for chains of length 200, 400, and 800 samples. Horizontal black lines mark the threshold of PSRF = 1.1, which is commonly accepted to indicate convergence. Each dot represents the PSRF value for one model parameter in HUGE associated with one of the 20 datasets

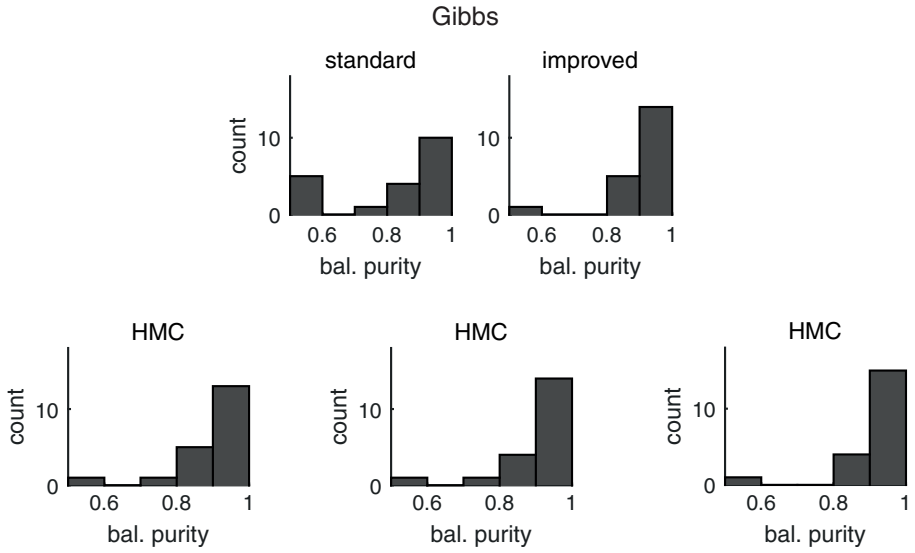

FIGURE 4 Top: Histograms over balanced purity values obtained with standard (left) and improved (right) Gibbs sampling. Bottom: Histograms over balanced purity values obtained with Hamiltonian Monte Carlo (HMC) for chains of length 200 (left), 400 (middle), and 800 (right)

histograms of the balanced purity over the datasets. In the comparison between standard and improved Gibbs sampler, we observe a clear improvement of the overall performance across the datasets.

In order to gain a better understanding of the failure mode of standard Gibbs, we chose one representative dataset and plotted the posterior estimates of subject assignment estimated for each chain

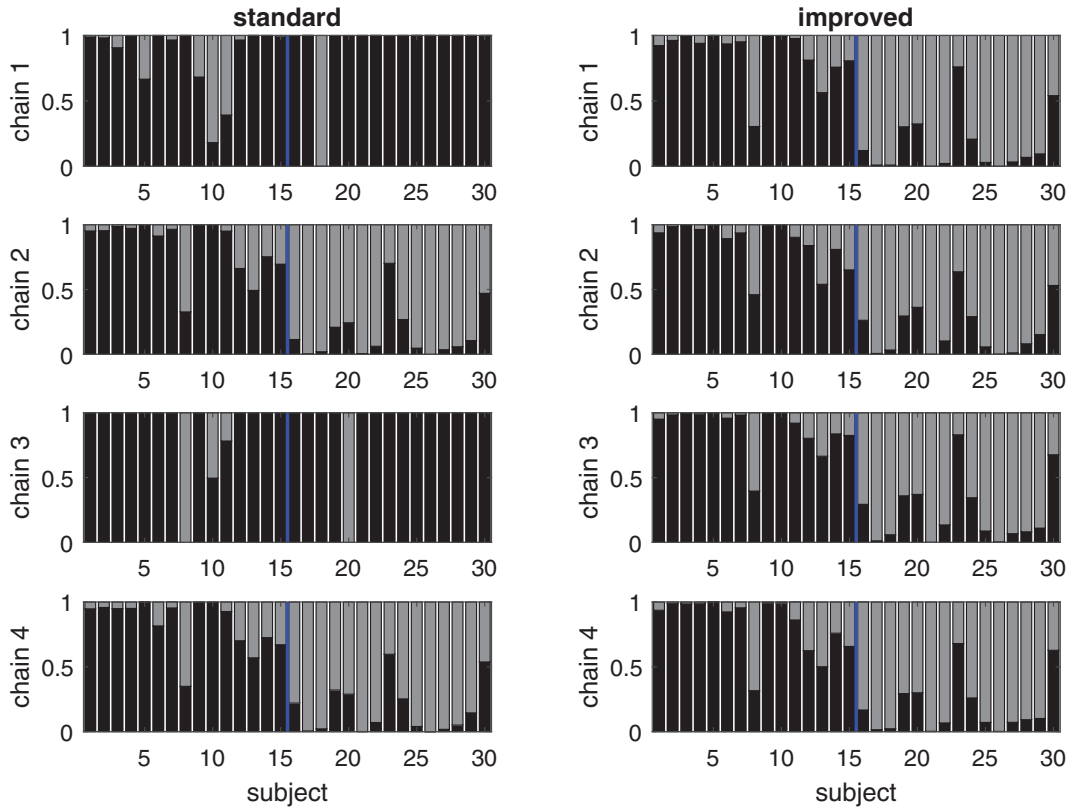

FIGURE 5 Posterior subject assignment for one exemplary synthetic dataset, estimated for each chain individually with standard (left) and improved (right) Gibbs sampling. The blue line separates the first 15 subject generated from the first cluster from the last 15 subjects generated from the second cluster

FIGURE 6 Mean log-joint probability of individual chains for the synthetic dataset in Figure 5 obtained with standard (left) and improved (right) Gibbs sampling

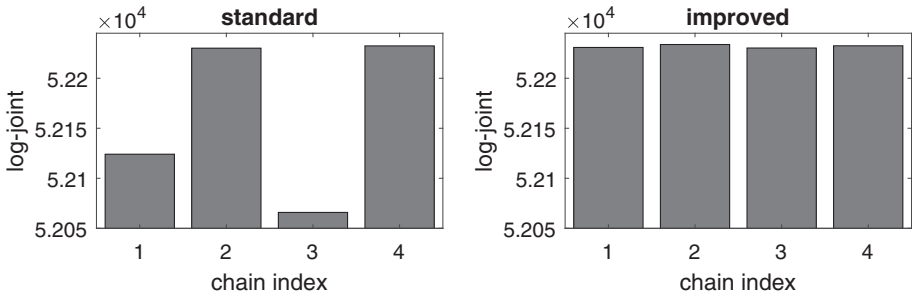

individually (Figure 5). This reveals that for standard Gibbs half of the chains (i.e., Chains 1 and 3) are stuck in a local maxima of the posterior density corresponding to an incorrect clustering. At the same time, Figure 6 shows a difference of over 100 in the mean log-joint probability between the chains. This indicates that Chains 1 and 3 are most likely stuck in low probability regions of the parameter space which are hard to get out of, for example, a local maximum in the posterior distribution. Conversely, for the improved version, all chains converged to the same area of the parameter space (Figure 5, right) with roughly the same mean log-joint probability (Figure 6, right). In addition, the estimated posterior subject assignment closely matches the ground truth assignment. Since the initial states of the chains are randomized, this result indicates that our improvements to the Gibbs sampler reduce the chance for chains to be trapped in local maxima of the posterior landscape.

In order to assess how well the model fits the data, we calculated the difference between the posterior samples of the predicted BOLD signal and the ground truth BOLD signal. Specifically, we used the DCM forward model to generate, for every posterior sample of the DCM parameters (after burn-in), the predicted BOLD response and calculated the root-mean-square error with respect to the ground-truth BOLD signal of the synthetic dataset. Figure 7 shows this error normalized by the *SD* of the ground-truth signal for the subjects of the same dataset shown in Figure 5. This plot reveals spikes in the error of certain subjects for the standard Gibbs sampler, while the improved sampler shows a uniformly low error. Interestingly, the

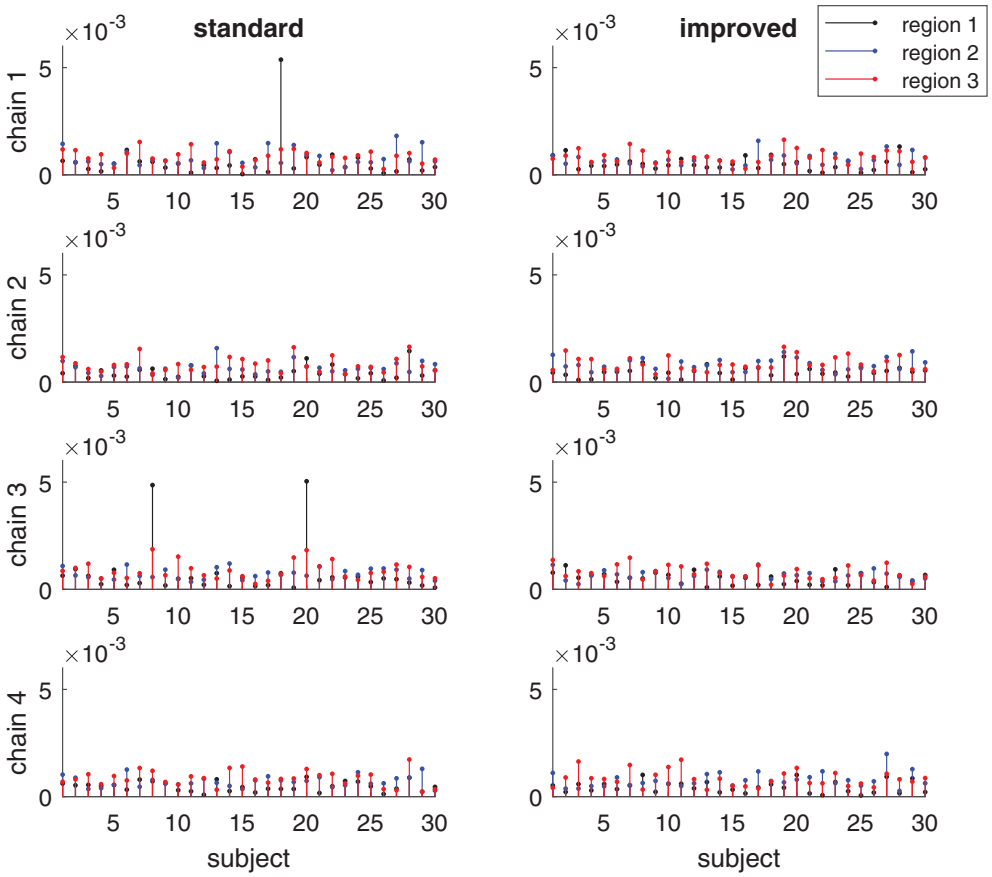

FIGURE 7 Per-subject normalized root mean square error between predicted BOLD response and ground truth BOLD signal for standard and improved Gibbs sampling for the same synthetic dataset shown in Figure 5

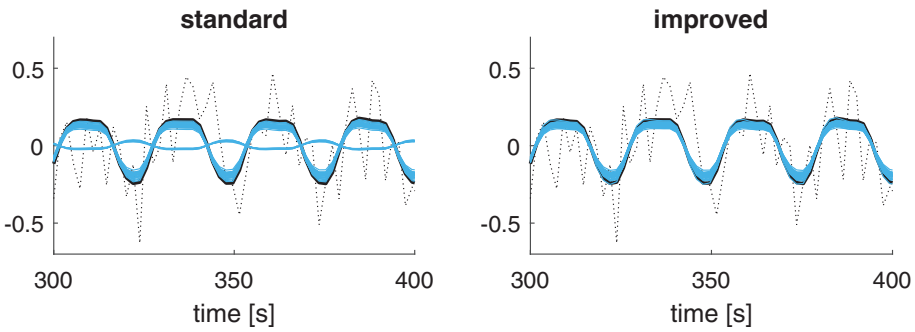

FIGURE 8 Comparison between posterior samples of the predicted BOLD response and the true, noise free BOLD signal for standard and improved Gibbs sampling. Data shown are for one region of subject 20 from the same synthetic dataset shown in Figure 5. Samples shown in blue are from all four chains

subjects showing high error (subjects 8, 18, and 20) seem to coincide with those subjects that are stuck in the wrong cluster in Figure 5. A visualization of posterior samples of the predicted BOLD response in Figure 8 reveals that the error seems to be because one chain converged to a parameter configuration leading to a poor prediction for the BOLD signal, possibly coupled with a high estimate for the variance of the measurement noise.

In order to compare our improved Gibbs sampler to HMC, we implemented the HUGE model in stan and inverted the model for each of the synthetic datasets. As with our Gibbs sampler, stan samples 4 independent chains per dataset, discards the first half of each chain for burn-in and pools the remaining samples over all chains to obtain convergence statistics and posterior quantiles. Since HMC has been designed for efficiency, HMC requires less samples to explore the target distribution than a sampler based on random-walk Monte Carlo. Hence, it is not appropriate to choose the same chain length for HMC and Gibbs sampling. Instead, a more sensible approach would be to run HMC until convergence, as assessed by the PSRF, and compare how many sample and how much computation time were required relative to Gibbs sampling. In time sensitive applications, which might arise, for example, in clinical settings, an alternative approach would be to allocate a time budget and compare which sampler is able to converge within this budget. Following this strategy, we repeated the entire experiment three times with three different setting for the chain length: 200, 400 and 800 samples. Based on preliminary experiments, we predicted that these settings would limit the

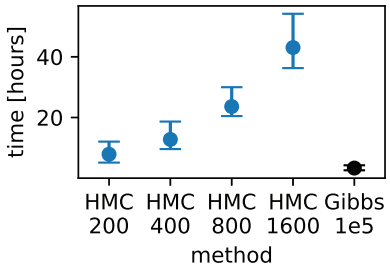

FIGURE 9 Comparison of the range of computation times for Hamiltonian Monte Carlo (HMC) (blue) and Gibbs sampling (black). HMC200: HMC with 200 samples, HMC400: HMC with 400 samples, HMC 800: HMC with 800 samples, and Gibbs1e5: Gibbs sampling with 10^5 samples

computation time to less than a day. For comparison, the Gibbs sampler converged within 3.5 hr on average.

The histograms over balanced purity values in Figure 4 show that, using chains of 800 samples, HMC achieved a similar clustering performance as our improved Gibbs sampler with 10^5 samples, confirming a superior efficiency per sample for HMC. However, Figure 3 reveals that the PSRFs are far from the value of 1, especially for the cluster mean and DCM connectivity parameters, indicating that the sampler has not converged, even for the maximum setting of 800 samples.

A simple solution would be to increase the length of the chains. Unfortunately, Figure 9 shows that even for the shortest chains of 200 samples, the computation time of HMC exceeds that of Gibbs sampling with 10^5 samples. Note that these experiments were conducted on a high performance computing (HPC) cluster equipped with processors which differ in speed. However, when repeating the sampling with HMC on a local workstation equipped with more powerful processors than the HPC cluster, we did not observe any significant speedup.

3.2 | Experiment 2: Experimental dataset

In the second experiment, we analysed a real-world dataset from an fMRI experiment investigating speech perception in stroke patients compared to healthy controls. The cohort included 26 healthy controls and 11 patients. For details of the experimental setup, see Leff et al. (2008). In a previous DCM-based analysis of this dataset (Schofield et al., 2012), a task-relevant network containing six regions (with three regions in either hemisphere) was identified. For hierarchical clustering, we simplified the network by removing two subcortical regions with low signal-to-noise ratio, resulting in the four-region network shown in Figure 10. This is in line with the approach from Yao et al. (2018).

As before, we inverted HUGE using both standard and improved Gibbs sampling and HMC. Settings were kept identical to the synthetic case except for the chain length, which was increased to 600,000 samples including 300,000 burn-in for Gibbs. The choice of

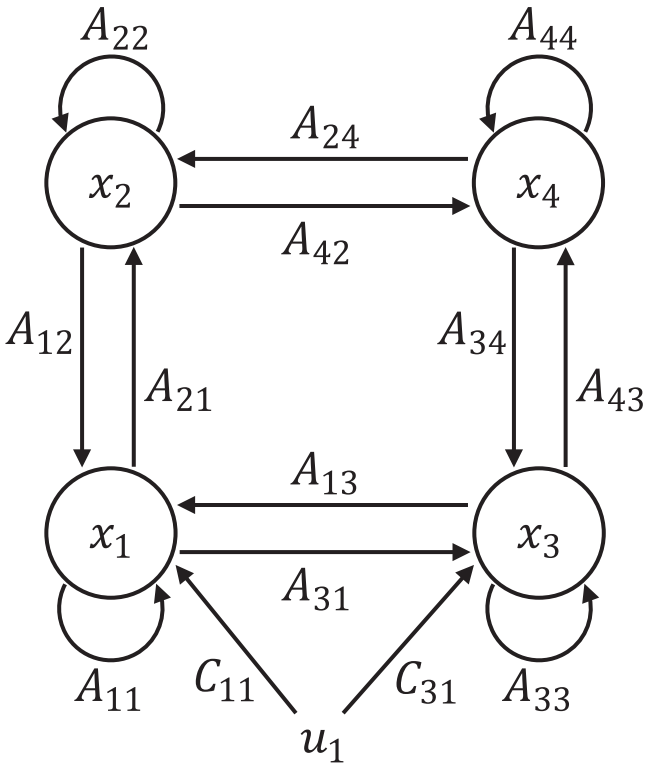

FIGURE 10 The four-region dynamic causal model (DCM) network structure used for the analysis of the experimental dataset

chain length was partly based on previous experience with a similar clustering model (Raman et al., 2016). Individual chains were sampled in parallel on an HPC cluster, with each chain having access to a single core. The HPC contains a variety of CPUs from different manufactures with clock speeds ranging from 2.3 to 3.7 GHz and jobs are assigned to a random node. A summary of the composition of the HPC can be found on its website (https://scicomp.ethz.ch/wiki/Euler). Sampling required 140×10^3 s (approx. 40 hr) on average for both versions of Gibbs sampling. Note that the computation time of the improved version of Gibbs is on average only 4% higher than that of standard Gibbs, indicating that the overhead introduced by our special proposal distributions is almost negligible. Also note that computation time is not a linear function of the number of regions of the DCM, but depends on many factors such as the number of connections, the number of subjects, the length of the time series, the type of the DCM (linear, bilinear, nonlinear), and so forth. However, the analysis from Section 2.4 showed that the complexity of the sampler does scale linearly with the number of subjects. This is relevant for applications involving large-scale datasets such as, for example, the Adolescent Brain Cognitive Development Study, the Human Connectome Project or the UK Biobank. Using this linear relation to extrapolate the computation time for this experiment to a dataset of 100 subjects, we would expect an average computation time of 105 hr (approx. 4.5 days), which is still less than the computation time of HMC for the present experiment. In this context, it is also important to note that for Gibbs sampling the subject related computations can be easily

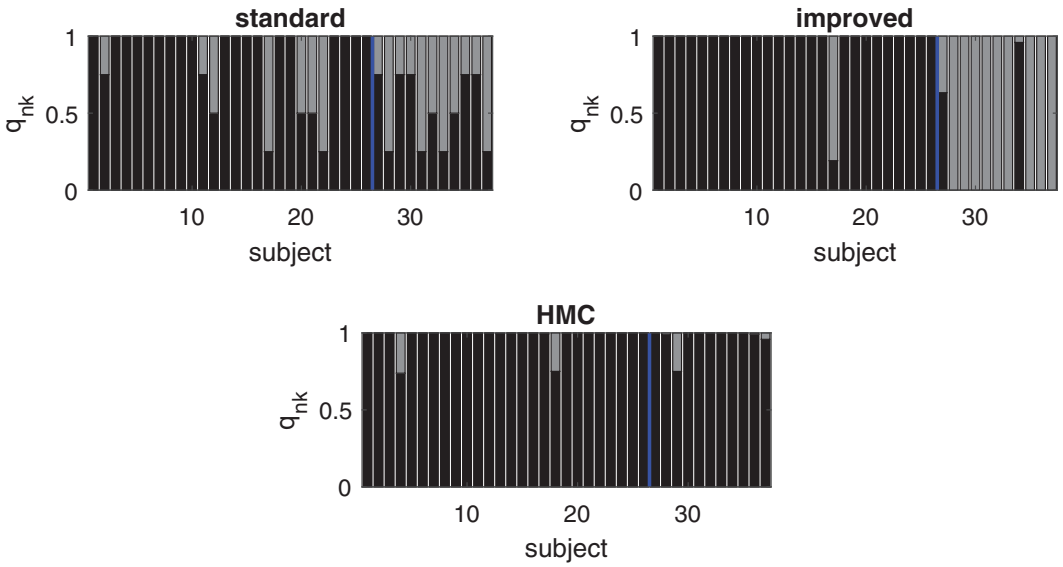

FIGURE 11 Subject assignment for Experiment 2, estimated from samples pooled over all chains. Top left: standard Gibbs, top right: improved Gibbs, bottom: Hamiltonian Monte Carlo (HMC). The blue line separates the controls (first 26 subjects) from patients (last 11 subjects)

parallelized, which could potentially reduce the computation time significantly if suitable hardware is available. In contrast, for HMC samplers, parallelization is less trivial since the simulation of the Hamiltonian dynamics is inherently sequential in nature.

Figure 11 shows the posterior assignment estimated from samples of all four chains. It is apparent that the clusters obtained with improved Gibbs sampling match far better onto the known subgroups of controls and patients. The balanced purity achieved with the improved method is 86%, whereas standard Gibbs sampling only achieves 60%. The reason for this difference becomes apparent when plotting the posterior assignment estimated for each chain individually. Figure 12 shows that, similar to Experiment 1, the chains from standard Gibbs are stuck in different local maxima of the posterior, while for the improved version, all chains converged to the same configuration. We again compared the mean log-joint probability between chains (Figure 13) and observed a difference of 100 for standard Gibbs and only 5 for the improved method.

Unlike the first experiment, there is no ground truth BOLD signal available for comparison. As an alternative, we compare the model prediction to the observed BOLD signal by analysing the squared difference between these signals for standard and improved Gibbs sampling. To this end, we obtain, for each subject, 10 equidistant samples from the posterior over DCM parameters from the post burn-in phase of each chain. The equidistant subsampling minimizes the correlation between samples. Each sample is used to generate a predicted BOLD signal, which in turn is used to calculate the squared difference to the observed signal. A Wilcoxon rank-sum test between all squared differences for standard and improved Gibbs samplers reveals that the median squared difference from samples obtained with standard Gibbs sampler is significantly higher than the median squared difference from samples obtained with improved sampler (p = .006). In addition, we also visualize the quality of model fit by plotting the mean log-likelihood of each chain for both standard and improved Gibbs sampling in Figure 14. Not only is the log-likelihood of the improved method higher, indicating a better model fit, but the log-likelihood values are also more consistent across chains for the improved sampler.

This observation is also reflected in the PSRF (Figure 15, top), which, for the improved sampler, lies below 1.1 for most parameters, with a few exceptions. On the other hand, for standard Gibbs, the PSRF of most parameters exceed 1.1, indicating poor convergence. Further convergence statistics like effective number of samples and autocorrelation times are reported in the Supplementary Material. Figure 16 shows a section of the sample trace for the cluster mean for both standard and improved Gibbs. Notice the lack of label switching, that is, the clusters switching places due to the symmetries of the clustering model, for standard Gibbs, which is another sign that the sampler is failing to explore the entirety of the posterior distribution.

In order to compare the performance of our improved Gibbs sampler to HMC on this real-world dataset, we used stan to invert HUGE for this dataset. Sampling 4 chains in parallel, each 200 samples long, with HMC took about 432×10^3 s (approx. 120 hr or 5 days). However, the posterior subject assignments and the PSRF shown in Figure 15 bottom, indicate that a chain length of 200 samples was not sufficient for convergence. Unfortunately, we were not able to repeat the experiment with longer chains, due to limitations on computation time on the HPC cluster used for the experiment.

It should be noted that the experimental dataset from this section has been analysed in Yao et al. (2018) using VB, which achieved a balanced purity of 91%. While this may seem to indicate that VB is more accurate than MCMC, it is important to note that, unlike for synthetic datasets, the known sub-groups of controls and patients in this experimental dataset only represent an external reference, instead of ground truth parameter settings of the model. In

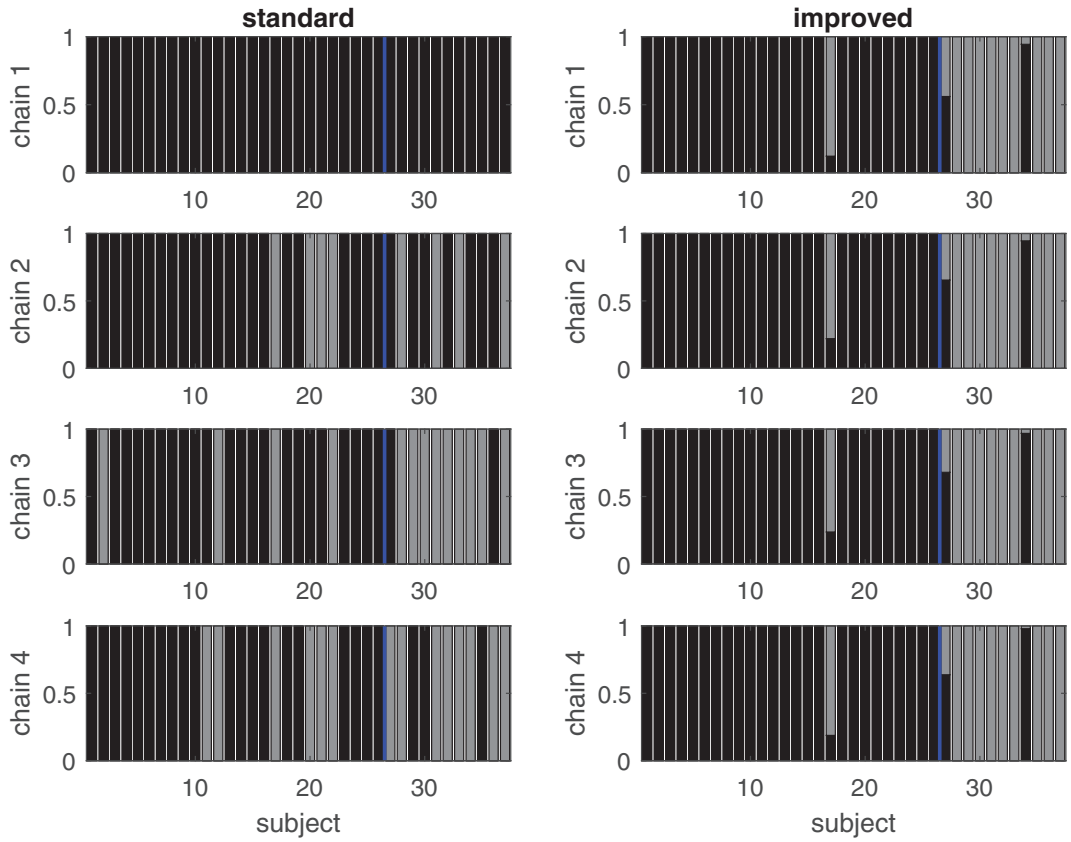

FIGURE 12 Subject assignment for Experiment 2, estimated for each chain individually for standard (left) and improved (right) Gibbs. The blue line separates the controls (first 26 subjects) from patients (last 11 subjects)

FIGURE 13 Mean log-joint probability of individual chains for standard (left) and improved (right) Gibbs sampling

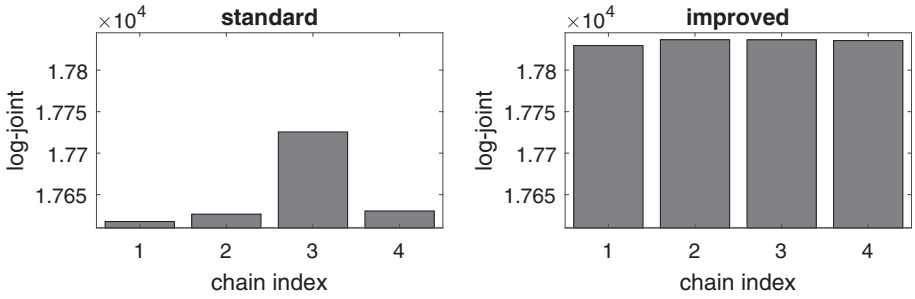

FIGURE 14 Mean log-likelihood of individual chains for standard (left) and improved (right) Gibbs sampling

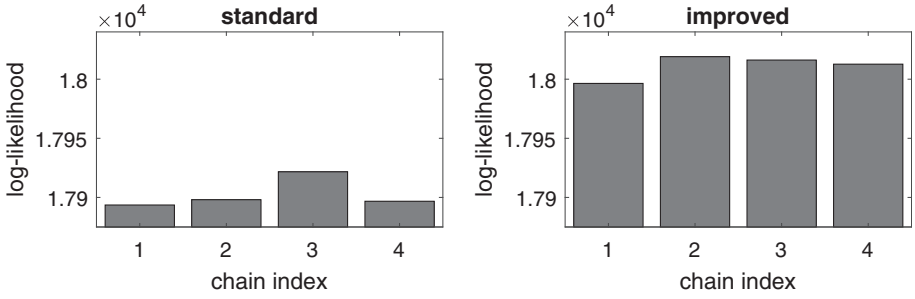

addition, a close inspection of the results reveals that the difference in balanced accuracy is due to a single subject (subject 27), who is assigned to the correct group by VB with high certainty, while the MCMC assignment for this subject is ambiguous, which may simply reflect the well-known tendency of VB to return overconfident results.

In order to gain more insight into why these subjects were assigned to the wrong cluster, we plot the posterior means of the subject-specific DCM parameters in Figure 17. This plot shows that the DCM parameters of two of the incorrectly assigned subjects were indeed consistent with the DCM parameters of the wrong group, while the parameter estimate for the third incorrectly assigned subject lies between the two groups. This indicates that the BOLD signals of these subjects simply lead to DCM parameter estimates that are consistent with the wrong cluster.

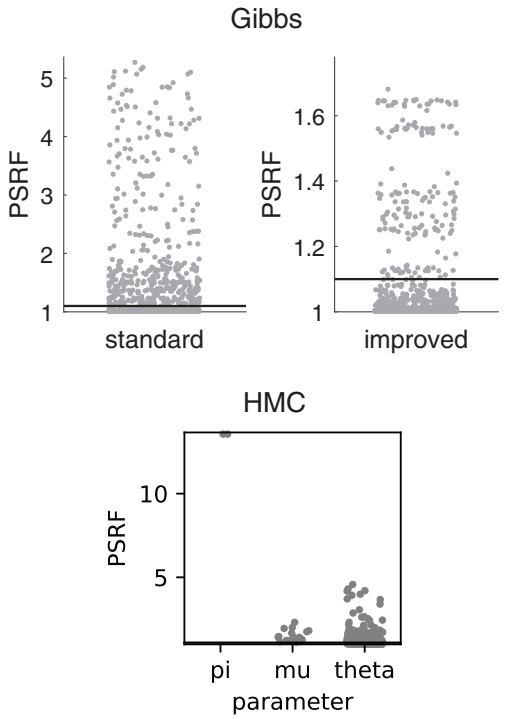

FIGURE 15 Top: Range of potential scale reduction factor (PSRF) values for standard (left) and improved (right) Gibbs for Experiment 2. Bottom: PSRF values for Hamiltonian Monte Carlo (HMC) with chain length of 200 for different parameter groups

4 | DISCUSSION

In this technical note, we introduced a set of proposal densities tailored to improving the convergence of MCMC samplers for hierarchical clustering. Comparing our approach to HMC in terms of computational complexity, the analysis in Section 2.4 showed no clear theoretical advantage for either method. In practice, computation time may vary depending on the particular application. Hence, we conducted extensive empirical tests on synthetic and real-world datasets, from which several conclusions can be drawn.

First, combining hierarchical clustering with dynamic system models such as DCM presents a formidable challenge to standard MCMC samplers due to the strong posterior correlation present, not only between clustering and DCM parameters, but also among the DCM parameters themselves. In addition, the inherent symmetries of clustering models induce multiple modes in the posterior.

Second, designing specialized proposal densities tailored to the specific challenges posed by the hierarchical clustering model represents an effective solution in practice, leading to better clustering performance in terms of balanced purity and also faster convergence. At the same time, the proposal densities we introduced in Section 2.2 have only a single free parameter (i.e., the mixing ratio between proposal distributions) which would need to be tuned for optimal performance.

Third, our experiments revealed that even state-of-the-art general purpose Monte Carlo methods, such as HMC, which were specifically designed to avoid random walk behaviour and efficiently sample from highly complex target distributions, struggle to converge reliably in timeframes as often required for solving computational problems (i.e., days). Despite being more efficient, that is, requiring fewer

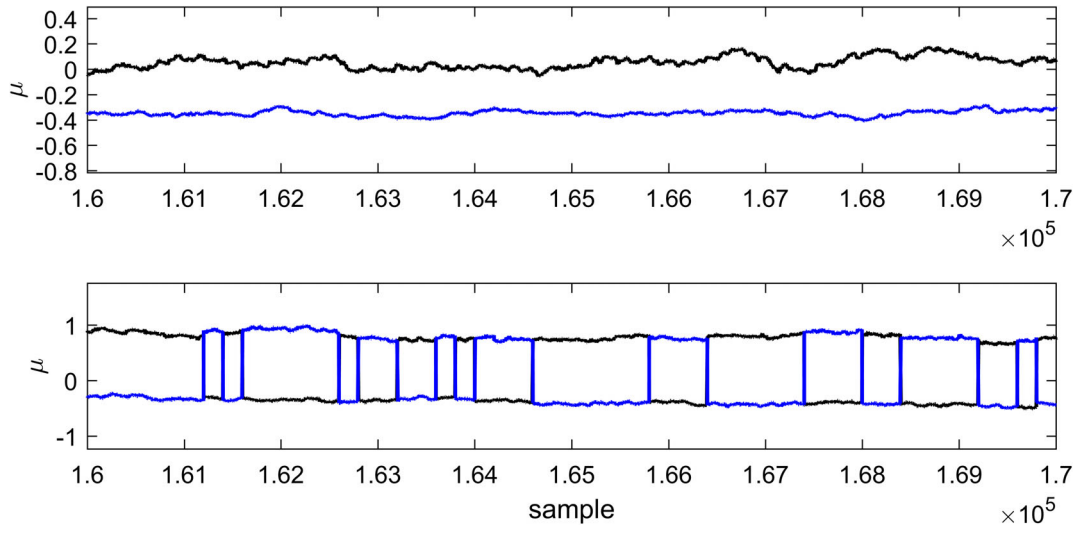

FIGURE 16 Sample trace for the cluster mean for standard (top) and improved (bottom) Gibbs

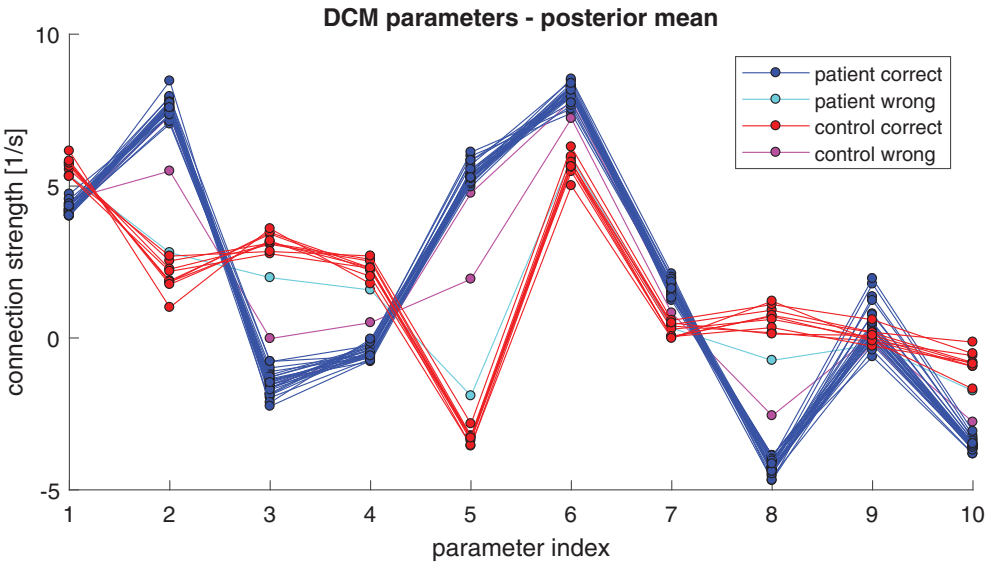

FIGURE 17 17Posterior mean of the subject-specific dynamic causal model (DCM) parameters obtained with the improved Gibbs sampler. The labels correct and wrong in the legend refer to the correctness of cluster assignment shown in Figure 11 top left. Specifically, control wrong refers to subject 17 and patient wrong to subjects 27 and 34, who were assigned to the wrong clusters

samples to explore the target distribution, HMC takes longer to run than Metropolized Gibbs sampling with our special purpose distributions and, for our empirical data, did not converge over the timeframe available on our local shared cluster (5 days). This indicates that, in practice, the overhead of having to simulate the Hamiltonian dynamics negate the advantage afforded by HMC of being able to obtain more independent samples.

Concerning the last point, it is important to note that we do not believe this observation to be a consequence of inefficient implementation, since we used the HMC implementation provided by stan, which translates the model into a C program and compiles it before running the sampler. This means that, in our experiments, the HMC sampler enjoyed the run time advantages of a compiled language, while our Gibbs sampler was implemented in MATLAB, with only the numerical integration of the DCM evolution equation being implemented in C. For both methods, individual chains were run in parallel.

Fourth, we would like to note that, although we have tested our improved Gibbs sampler on HUGE, which is a DCM for fMRI-based hierarchical clustering model, our proposed approach can be extended easily to hierarchical clustering based on other generative models or other DCM variants, such as DCM for EEG. Clearly, in contrast to the HMC sampler in stan (and samplers provided by other toolboxes), our approach does not generalize across models; instead, the proposal densities need to be adapted to the specific model used. However, as demonstrated above, an analysis of the dependency structure in the overall hierarchical clustering model provides guidance for this relatively straightforward step.

Compared to Yao et al. (2018), the MCMC-based approach presented here offers conceptual and practical advantages, which complement VB-based model inversion. Due to its asymptotic exactness, MCMC may be used as a principled way to guard against estimation errors of VB which arise from multi-modal posteriors or local minima in the objective function. Concretely, one could use VB to quickly obtain a preliminary result and proceed with further analysis while running MCMC to confirm that the clustering found with VB is not, for example, due to a local minimum in the free energy landscape. On the practical side, MCMC is more flexible when it comes to modifications of the model, while for VB even seemingly trivial modifications such as choosing a different prior distribution would require rederiving the update equations, which represents a major effort. This point is of particular importance since the model will be released as open-source software, allowing interested users to introduce their own modifications.

Clustering subjects of heterogeneous populations is finding increasing application in neuroimaging, particularly in application to psychiatry (Brodersen et al., 2014; Dinga et al., 2019; Drysdale et al., 2017; Feczko et al., 2018; Feczko et al., 2019; Marquand, Wolfers, Mennes, Buitelaar, & Beckmann, 2016; Wolfers et al., 2019), where the considerable heterogeneity of diseases according to current classifications represents a central problem (Stephan et al., 2016). The ability to detect unknown subgroups could greatly improve our means of stratifying psychiatric populations and conduct more powerful clinical trials. This is particularly the case when subgroups are not simply defined in terms of data features, but are interpretable in terms of physiological processes that generated the data—a main motivation behind hierarchical formulations of GE. The technical improvement proposed in this article may find useful application in future studies that utilize GE for a stratification of heterogeneous disorders.

ACKNOWLEDGEMENTS

The work presented in this article has been funded by the René und Susanne Braginsky Foundation and the University of Zurich (to K. E. S.). The authors would like to thank Prof Alex Leff for his generous permission to use the fMRI speech perception dataset.

CONFLICTS OF INTEREST

The authors declare no conflicts of interest.

DATA AVAILABILITY STATEMENT

The synthetic data used in Section 3.1 will be deposited on the ETH Research Collection (https://www.research-collection.ethz.ch/), an open repository that complies with the FAIR principles. The experimental dataset used in Section 3.2 can be obtained, on reasonable request, from Prof Alex Leff, University College London.

ORCID

Yu Yao https://orcid.org/0000-0001-7658-3503

REFERENCES

Ahn, W.-Y., Haines, N., & Zhang, L. (2017). Revealing neurocomputational mechanisms of reinforcement learning and decision-making with the hBayesDM package. *Computational Psychiatry*, *1*, 24–57. https://doi.org/10.1162/CPSY_a_00002

Baydin, G. A., Pearlmutter, B. A., Radul, A. A., & Siskind, M. J. (2018). Automatic differentiation in machine learning: A survey. *Journal of Machine Learning Research*, *18*, 1–43.

Behrens, G., Friel, N., & Hurn, M. (2012). Tuning tempered transitions. *Statistics and Computing*, *22*(1), 65–78. https://doi.org/10.1007/s11222-010-9206-z

Betancourt, M. (2016). Identifying the optimal integration time in Hamiltonian Monte Carlo.

Betancourt, M., & Girolami, M. (2015). Hamiltonian Monte Carlo for hierarchical models. In S. K. Upandhyay, U. Singh, D. K. Dey, & A. Loganathan (Eds.), *Current trends in Bayesian methodology with applications*. New York, NY: Chapman and Hall.

Bishop, C. (2006). *Pattern recognition and machine learning*. Cambridge: Springer.

Brodersen, K. H., Deserno, L., Schlagenhauf, F., Lin, Z., Penny, W., Buhmann, J. M., & Stephan, K. E. (2014). Dissecting psychiatric spectrum disorders by generative embedding. *NeuroImage: Clinical*, *4*, 98–111. https://doi.org/10.1016/j.nicl.2013.11.002

Brodersen, K. H., Schofield, T. M., Leff, A. P., Ong, C. S., Lomakina, E. I., Buhmann, J. M., & Stephan, K. E. (2011). Generative embedding for model-based classification of fMRI data. *PLoS Computational Biology*, *7*(6), e1002079. https://doi.org/10.1371/journal.pcbi.1002079

Brooks, S., & Gelman, A. (1998). General methods for monitoring convergence of iterative simulations. *Journal of Computational and Graphical Statistics*, *7*(4), 434–455. https://doi.org/10.1080/10618600.1998.10474787

Brooks, S., Gelman, A., Jones, G., & Meng, X. L. (2011). In S. Brooks, A. Gelman, G. Jones, & X. L. Meng (Eds.), *Handbook of Markov chain Monte Carlo*. New York, NY: Chapman & Hall.

Calderhead, B., & Girolami, M. (2009). Estimating Bayes factors via thermodynamic integration and population MCMC. *Computational Statistics & Data Analysis*, *53*, 4028–4045. https://doi.org/10.1016/j.csda.2009.07.025

Calderhead, B., & Girolami, M. (2011). Statistical analysis of nonlinear dynamical systems using differential geometric sampling methods. *Journal of the Royal Society Interface Focus*, *1*(6), 821–835. https://doi.org/10.1098/rsfs.2011.0051

Calderhead, B., Girolami, M., & Lawrence, N. D. (2009). Accelerating Bayesian inference over nonlinear differential equations with Gaussian processes. In (pp. 217-224).

Carlin, B. P., & Chib, S. (1995). Bayesian model choice via Markov chain Monte Carlo methods. *Journal of the Royal Statistical Society. Series B (Methodological)*, *57*(3), 473–484. https://doi.org/10.1111/j.2517-6161.1995.tb02042.x

David, O., Kiebel, S. J., Harrison, L. M., Mattout, J., Kilner, J. M., & Friston, K. J. (2006). Dynamic causal modeling of evoked responses in EEG and MEG. *NeuroImage*, *30*(4), 1255–1272. https://doi.org/10.1016/j.neuroimage.2005.10.045

Dinga, R., Schmaal, L., Penninx, B. W. J. H., van Tol, M. J., Veltman, D. J., van Velzen, L., … Marquand, A. F. (2019). Evaluating the evidence for biotypes of depression: Methodological replication and extension of Drysdale et al. (2017). *NeuroImage: Clinical*, *22*, 101796. https://doi.org/10.1016/j.nicl.2019.101796

Drysdale, A. T., Grosenick, L., Downar, J., Dunlop, K., Mansouri, F., Meng, Y., … Liston, C. (2017). Resting-state connectivity biomarkers define neurophysiological subtypes of depression. *Nature Medicine*, *23*(1), 28–38. https://doi.org/10.1038/nm.4246

Duane, S., Kennedy, A. D., Pendleton, B. J., & Roweth, D. (1987). Hybrid Monte Carlo. *Physics Letters B*, *195*(2), 216–222. https://doi.org/10.1016/0370-2693(87)91197-X

Feczko, E., Balba, N. M., Miranda-Dominguez, O., Cordova, M., Karalunas, S. L., Irwin, L., … Fair, D. A. (2018). Subtyping cognitive profiles in autism spectrum disorder using a functional random forest algorithm. *NeuroImage*, *172*, 674–688. https://doi.org/10.1016/j.neuroimage.2017.12.044

Feczko, E., Miranda-Dominguez, O., Marr, M., Graham, A. M., Nigg, J. T., & Fair, D. A. (2019). The heterogeneity problem: Approaches to identify psychiatric subtypes. *Trends in Cognitive Sciences*, *23*(7), 584–601. https://doi.org/10.1016/j.tics.2019.03.009

Frässle, S., Yao, Y., Schöbi, D., Aponte, E. A., Heinzle, J., & Stephan, K. E. (2018). Generative models for clinical applications in computational psychiatry. *Wiley Interdisciplinary Reviews: Cognitive Science*, *9*(3), e1460. https://doi.org/10.1002/wcs.1460

Friston, K. J., Harrison, L., & Penny, W. (2003). Dynamic causal modelling. *NeuroImage*, *19*(4), 1273–1302. https://doi.org/10.1016/S1053-8119(03)00202-7

Friston, K. J., Litvak, V., Oswal, A., Razi, A., Stephan, K. E., van Wijk, B. C. M., … Zeidman, P. (2016). Bayesian model reduction and empirical Bayes for group (DCM) studies. *NeuroImage*, *128*(Suppl C), 413–431. https://doi.org/10.1016/j.neuroimage.2015.11.015

Friston, K. J., Mattout, J., Trujillo-Barreto, N., Ashburner, J., & Penny, W. (2007). Variational free energy and the Laplace approximation. *NeuroImage*, *34*(1), 220–234. https://doi.org/10.1016/j.neuroimage.2006.08.035

Friston, K. J., Mechelli, A., Turner, R., & Price, C. J. (2000). Nonlinear responses in fMRI: The balloon model, Volterra kernels, and other hemodynamics. *NeuroImage*, *12*(4), 466–477. https://doi.org/10.1006/nimg.2000.0630

Gelman, A. (2014). *Bayesian data analysis* (3rd ed.). Boca Raton, FL: CRC Press.

Green, P. J. (1995). Reversible jump Markov chain Monte Carlo computation and Bayesian model determination. *Biometrika*, *82*(4), 711–732. https://doi.org/10.2307/2337340

Gutenkunst, R. N., Waterfall, J. J., Casey, F. P., Brown, K. S., Myers, C. R., & Sethna, J. P. (2007). Universally sloppy parameter sensitivities in systems biology models. *PLoS Computational Biology*, *3*(10), e189. https://doi.org/10.1371/journal.pcbi.0030189

Hoffman, M. D., & Gelman, A. (2014). The no-U-turn sampler: Adaptively setting path lengths in Hamiltonian Monte Carlo. *Journal of Machine Learning Research*, *15*, 1593–1623.

Kramer, A., Calderhead, B., & Radde, N. (2014). Hamiltonian Monte Carlo methods for efficient parameter estimation in steady state dynamical systems. *BMC Bioinformatics*, *15*(1), 253. https://doi.org/10.1186/1471-2105-15-253

Leff, A. P., Schofield, T. M., Stephan, K. E., Crinion, J. T., Friston, K. J., & Price, C. J. (2008). The cortical dynamics of intelligible speech. *The Journal of Neuroscience*, *28*(49), 13209–13215. https://doi.org/10.1523/jneurosci.2903-08.2008

Marquand, A. F., Wolfers, T., Mennes, M., Buitelaar, J., & Beckmann, C. F. (2016). Beyond lumping and splitting: A review of computational approaches for stratifying psychiatric disorders. *Biological Psychiatry: Cognitive Neuroscience and Neuroimaging*, *1*(5), 433–447. https://doi.org/10.1016/j.bpsc.2016.04.002

Meeds, T., Roeder, G., Grant, P., Phillips, A., & Dalchau, N. (2019). *Efficient amortised Bayesian inference for hierarchical and nonlinear dynamical systems*. Paper presented at the Proceedings of the 36th International Conference on Machine Learning, Proceedings of Machine Learning Research.

Owen, M. J. (2014). New approaches to psychiatric diagnostic classification. *Neuron*, *84*(3), 564–571. https://doi.org/10.1016/j.neuron.2014.10.028

Raman, S., Deserno, L., Schlagenhauf, F., & Stephan, K. E. (2016). A hierarchical model for integrating unsupervised generative embedding and empirical Bayes. *Journal of Neuroscience Methods*, *269*, 6–20. https://doi.org/10.1016/j.jneumeth.2016.04.022

Schofield, T. M., Penny, W., Stephan, K. E., Crinion, J. T., Thompson, A. J., Price, C. J., & Leff, A. P. (2012). Changes in auditory feedback connections determine the severity of speech processing deficits after stroke. *The Journal of Neuroscience*, *32*(12), 4260–4270. https://doi.org/10.1523/jneurosci.4670-11.2012

Schumann, G., Binder, E. B., Holte, A., de Kloet, E. R., Oedegaard, K. J., Robbins, T. W., … Wittchen, H. U. (2014). Stratified medicine for mental disorders. *European Neuropsychopharmacology*, *24*(1), 5–50. https://doi.org/10.1016/j.euroneuro.2013.09.010

Stan Development Team. (2020). *Stan reference manual*. Retrieved from https://mc-stan.org

Stephan, K. E., Bach, D. R., Fletcher, P. C., Flint, J., Frank, M. J., Friston, K. J., … Breakspear, M. (2016). Charting the landscape of priority problems in psychiatry, part 1: Classification and diagnosis. *Lancet Psychiatry*, *3*(1), 77–83. https://doi.org/10.1016/s2215-0366(15)00361-2

Stephan, K. E., Schlagenhauf, F., Huys, Q. J. M., Raman, S., Aponte, E. A., Brodersen, K. H., … Heinz, A. (2017). Computational neuroimaging strategies for single patient predictions. *NeuroImage*, *145*(Pt B), 180–199. https://doi.org/10.1016/j.neuroimage.2016.06.038

Stephan, K. E., Weiskopf, N., Drysdale, P. M., Robinson, P. A., & Friston, K. J. (2007). Comparing hemodynamic models with DCM. *NeuroImage*, *38*(3), 387–401. https://doi.org/10.1016/j.neuroimage.2007.07.040

Stephens, M. (2000). Dealing with label switching in mixture models. *Journal of the Royal Statistical Society Series B (Statistical Methodology)*, *62*, 795–809. https://doi.org/10.1111/1467-9868.00265

Translational Neuromodeling Unit. (2014). TAPAS - Translational Algorithms for Psychiatry-Advancing Science. Retrieved from http://www.translationalneuromodeling.org/tapas

van Leeuwen, T. M., den Ouden, H. E. M., & Hagoort, P. (2011). Effective connectivity determines the nature of subjective experience in grapheme-color synesthesia. *The Journal of Neuroscience*, *31*(27), 9879–9884. https://doi.org/10.1523/jneurosci.0569-11.2011

Wenk, P., Gotovos, A., Bauer, S., Gorbach, N. S., Krause, A., & Buhmann, J. M. (2019). *Fast Gaussian process based gradient matching for parameter identification in systems of nonlinear ODEs*. Paper presented at the Proceedings of Machine Learning Research, Proceedings of Machine Learning Research.

Wolfers, T., Floris, D. L., Dinga, R., van Rooij, D., Isakoglou, C., Kia, S. M., … Beckmann, C. F. (2019). From pattern classification to stratification: Towards conceptualizing the heterogeneity of autism spectrum disorder. *Neuroscience & Biobehavioral Reviews*, *104*, 240–254. https://doi.org/10.1016/j.neubiorev.2019.07.010

Xun, X., Cao, J., Mallick, B., Maity, A., & Carroll, R. J. (2013). Parameter estimation of partial differential equation models. *Journal of the American Statistical Association*, *108*(503), 1009–1020. https://doi.org/10.1080/01621459.2013.794730

Yao, Y., Raman, S. S., Schiek, M., Leff, A., Frässle, S., & Stephan, K. E. (2018). Variational Bayesian inversion for hierarchical unsupervised generative embedding (HUGE). *NeuroImage*, *179*, 604–619. https://doi.org/10.1016/j.neuroimage.2018.06.073

SUPPORTING INFORMATION

Additional supporting information may be found online in the Supporting Information section at the end of this article.

How to cite this article: Yao Y, Stephan KE. Markov chain Monte Carlo methods for hierarchical clustering of dynamic causal models. *Hum Brain Mapp*. 2021;42:2973–2989. https://doi.org/10.1002/hbm.25431